Catalysis Today 339 (2020) 265–273

Contents lists available at ScienceDirect

Catalysis Today

journal homepage: www.elsevier.com/locate/cattod

Study on the crystal plane effect of CuO/TiO_2 catalysts in NH_3-SCR reaction

Shuohan Yu[a,b], Yiyang Lu[a,b], Fei Gao[a,b], Lin Dong[a,b,*]

[a] Jiangsu Key Laboratory of Vehicle Emissions Control, School of the Environment, Center of Modern Analysis, Nanjing University, Nanjing 210093, PR China
[b] Key Laboratory of Mesoscopic Chemistry of MOE, School of Chemistry and Chemical Engineering, Nanjing University, Nanjing 210093, PR China

ARTICLE INFO

Keywords:
NH_3-SCR
TiO_2
Cu oxide
Exposed facets

ABSTRACT

In this work, TiO_2 nano-octahedron and nano-rods were successfully synthesized, and Cu oxides were loaded on them. Structures of CuO/TiO_2 catalysts were studied by XRD, TEM, and Raman techniques. It was founded that TiO_2 nano-octahedron and nano-rods dominantly exposed (101) and (100) facets of TiO_2, respectively. Cu cations located in tetrahedral vacant sites on (101) facet of TiO_2 and coordinated with 4 neighbor oxygen, whereas it located in octahedral vacant sites on (100) facet of TiO_2 and coordinated with 6 neighbor oxygen, which resulted in redox cycle $Cu^{2+} + Ti^{3+} \longleftrightarrow Cu^{+} + Ti^{4+}$ and more acid sites on surface of CuO/TiO_2 nano-octahedron, and thus the enhanced NH_3-SCR performance.

1. Introduction

Selective catalytic reduction (SCR) technology has been used worldwide for the control of NO_x emissions in exhaust gases from stationary sources and automobiles. Among the reducing agents can be utilized in SCR, ammonia has been adopted in general, which is called NH_3-SCR [1–4]. Recently, numerous NH_3-SCR catalysts such as Cu [5–9], Mn [2,10–14], V [15–17], Fe [18–20], Ce [2,11,21,22] based materials, has been reported to exhibit satisfactory catalytic activities. V_2O_5/TiO_2 is the most commonly used catalyst because of its high NO conversion, high thermal stability, and excellent anti-SO_2 poisoning ability [15–17]. Some of V based catalysts have been commercialized. Despite these achievements, the narrow operation temperature window, as well as the volatility and toxicity of VO_x, inhibits its enormous application [23–25]. MnO_x and other manganese-containing catalysts present promising NO_x conversions in the range 100–200 °C. However, improvement N_2 selectivity and poisoning resistance to H_2O and sulfur oxides at low temperatures is important for low temperature application [26–28].

Alternatively, copper-containing catalysts, mostly in the form of Cu exchanged zeolites such as Cu/SAPO-34 [29–31], also show superior low temperature activity. Due to the high cost of copper exchanged zeolites, copper-containing mixed oxide catalysts have also been developed. According to Weng's report [32], CuO_x impregnated on the co-precipitated WO_3-ZrO_2 support shows high SCR activity in the range 200–320 °C. The acidity of the WO_3-ZrO_2 support allows to improve ammonia adsorption, essential for high SCR activity. Sullivan et al. [33,34] reported that copper oxide based catalysts prepared from two different precursors ($Cu(NO_3)_2$ and $CuSO_4$) with various oxide supports (SiO_2, TiO_2 and Al_2O_3) are also active in the NH_3-SCR reaction. Other copper based catalysts, such as CuMnAl [35] and CuNb [36], also show remarkable NH_3-SCR activities between 200 and 300 °C.

In recent years, the facet-dependent catalysis [37,38] has exerted a tremendous scientific and technological fascination. Song [39] and co-workers studied the influence of exposed (001) facet of TiO_2 support on NH_3-SCR performances of V_2O_5/TiO_2 catalysts. They compared two TiO_2 supports including commercial P25 and TiO_2 nano-sheets exposed (001) facet of TiO_2. They found that V_2O_5/TiO_2 nano-sheets had strong interaction with active V species, which resulted in enhanced redox ability, and thus, improved NH_3-SCR activity of V_2O_5/TiO_2 nano-sheets. Deng [40] and co-workers studied the NH_3-SCR performances of Mn loaded on TiO_2 exposed (001) and (101) facets. MnO_x could be highly dispersed on (001) facet of TiO_2, which brought more acid sites on catalyst surfaces, and thus, enhanced the NH_3-SCR performances of catalysts. Shen et al. [41] found that V species on different exposed facets of TiO_2 support had different coordination structure, which resulted that V_2O_5 loaded on (001) facet of TiO_2 exhibited better NH_3-SCR activity than V_2O_5 loaded on (101) facet of TiO_2. Owing to the simple and clear structure of materials with dominant exposed facets, the study of facet-dependent catalysis would be helpful to understand the influences of loading metal oxides, supports, and interaction between them on NH_3-SCR performance.

Our group has focused on the study of Cu dispersion on various supports for several years [42–46], such as Al_2O_3, TiO_2, and CeO_2. It

* Corresponding author at: Jiangsu Key Laboratory of Vehicle Emissions Control, School of the Environment, Center of Modern Analysis, Nanjing University, Nanjing 210093, PR China.
E-mail address: donglin@nju.edu.cn (L. Dong).

https://doi.org/10.1016/j.cattod.2019.04.051
Received 23 December 2018; Received in revised form 28 March 2019; Accepted 14 April 2019
Available online 15 April 2019
0920-5861/

was found that the catalytic activity of Cu based catalysts were highly depended on the dispersion state of Cu species. A method to estimate the loading metal dispersion capacity on surfaces of materials was provided [46,47]. In addition, we developed a simple method to synthesize TiO_2 with certain morphology [48]. In the present work, we studied the Cu ion dispersion on (100) and (101) facets of TiO_2 by loading copper oxides on TiO_2 nano-octahedrons and nano-rods. In addition, their effects on NH_3-SCR performances were also investigated.

2. Experimental details

TiO_2 supports with certain morphologies were synthesized according to Liu's method [48]. All the agents were purchased form Aladdin, and were used without further purifying.

2.1. Preparation of $Ti(OH)_4$ precursor

Concentrated hydrochloric acid (2 mL) was dissolved in 50 mL deionized water under magnetic stirring. $TiCl_4$ (6.6 mL) was added the solution dropwise under ice-water bath. Diluted ammonium hydroxide (concentrated ammonium hydroxide: deionized water = 1:4) was added into the obtained solution until pH reached 9. The obtained suspension was kept stirring for 2 h at room temperature. The suspension was washed by water and was centrifugal separated until no Cl^- ions could be detected by $AgNO_3$ solution in the eluate. The obtained white sediment was $Ti(OH)_4$ precursor.

2.2. Preparation of TiO_2 nano-octahedrons

$Ti(OH)_4$ precursor was dispersed in a solution containing 0.2 g NH_4Cl, 15 mL deionized water, and 15 mL isopropanol. The mixture was transferred into a Teflon-lined stainless steel autoclave and heated at 180 °C for 36 h. The products were separated by centrifugation and were washed with deionized water and ethanol for 3 times, respectively. The obtained powders were dried at 70 °C overnight, and were calcined at 450 °C for 3 h. The calcined sample was named as TiO_2-NOs.

2.3. Preparation of TiO_2 nano-rods

$Ti(OH)_4$ precursor was dispersed in a solution containing 0.5 g $(NH_4)_2SO_4$, 15 mL deionized water, and 15 mL isopropanol. The mixture was transferred into a Teflon-lined stainless steel autoclave and heated at 180 °C for 36 h. The products were separated by centrifugation and were washed with deionized water and ethanol for 3 times, respectively. The obtained powders were dried at 70 °C overnight, and were calcined at 450 °C for 3 h. The calcined sample was named as TiO_2-NRs.

2.4. Preparation of CuO supported TiO_2 with different shapes

CuO was supported on TiO_2 by impregnation method. TiO_2 powder was impregnated in solution containing certain amount of $Cu(Ac)_2$ (0.6 mmol Cu per 100 m^2 TiO_2, surface areas of TiO_2 supports were showed in Table S1). The mixture was water-bathed heated at 80 °C until all the water in the mixture was removed. The obtained powders were dried at 100 °C overnight, and was calcined at 450 °C in air for 3 h. The final samples was named as 06CuO/TiO_2-NOs for CuO supported TiO_2 nano-octahedrons, and 06CuO/TiO_2-NRs for CuO supported TiO_2 nano-rods.

2.5. Characterizations

X-ray diffraction (XRD) patterns were recorded on a Philips X'pert Pro diffractometer using Ni-filtered Cu Ka radiation (0.15418 nm). The X-ray tube was operated at 40 kV and 40 mA.

Brunauer–Emmet–Teller (BET) surface area was measured by nitrogen adsorption at 77 K on a Micrometrics ASAP-2020 adsorption apparatus.

Laser Raman spectra (LRS) were recorded by using Renishaw Invia spectrometer. Raman excitation at 514.5 nm was provided by Ar^+ laser. A laser power of 20 mW was applied.

H_2-temperature-programmed reduction (TPR) was carried out in a quartz U-tube reactor connected to a thermal conduction detector with H_2–Ar mixture (7.3% H_2 by volume) as reductant. 50.0 mg of sample was used for each measurement. Before switched to the H_2–Ar stream, the sample was pretreated in a N_2 stream at 300 °C for 1 h. TPR started from room temperature at a rate of 10 C min^{-1}.

X-ray photoelectron spectroscopy (XPS) analysis was performed on a PHI 5000 Versaprobe system, using Al Ka radiation (1486.6 eV) operating at an accelerating power of 150 W. All binding energies (BEs) were referenced to the C 1 s peak at 284.6 eV. This reference gave BE values with an accuracy at ± 0.1 eV

TEM analysis was performed on a TF-20 transmission electron microscope. X-ray energy dispersive spectroscopy (EDS) mappings were acquired using the Super-X EDS system which is composed of four silicon drift detector covering 0.7 s rad collection.

The in situ DRIFT experiments were performed on a Nicolet Nexus 5700 FTIR spectrometer by using a diffuse reflectance attachment (HARRICK) equipped with a reaction cell (ZnSe windows). The number of scans was 32 at a resolution of 4 cm^{-1} and the spectra were presented as Kubelka–Munk function referred to background spectra recorded catalyst in N_2.

2.6. Catalytic activity tests

The NH_3-SCR activity tests were performed in a fixed-bed reactor with 0.2 g catalyst. The feed gas contained 500 ppm NO, 500 ppm NH_3, 5 vol.% O_2 with N_2 as the balance gas. The total flow rate of the feed gas was 100 mL/min, corresponding to a space velocity approximately 30,000 h^{-1}. Including NO, NH_3, NO_2, and N_2O, the effluent gases were continuously analyzed at 150 °C by an online Thermofisher IS10 FTIR spectrometer equipped with a 2 m path-length gas cell (250 ml volume).

3. Results and discussions

3.1. Structure of TiO_2 supports and CuO/TiO_2 catalysts

TEM analysis was employed to investigate the morphology of TiO_2-NOs and TiO_2-NRs samples. As it was displayed in Figs. 1a and S1, TiO_2-NOs exhibits octahedron shape with an average width of 22 nm and an average length of 30 nm. According to the close-up image of TiO_2-NOs (Fig. 1c), TiO_2 lattice fringe of d = 0.35 nm is observed, corresponding to the anatase TiO_2 (101) crystal plane. This group of lattice fringe is parallel to the exposed facet of TiO_2-NOs, which demonstrates that TiO_2-NOs exposed (101) facet dominantly. In Figs. 1b and S1, TiO_2-NRs sample exhibits nano-rods shape with an average width of 17 nm and an average length of 28 nm. In the close-up image of TiO_2-NRs (Fig. 1d), TiO_2 lattice fringe of d = 0.19 nm is observed, corresponding to the anatase TiO_2 (100) crystal plane. This group of lattice fringe is parallel to the long edge of TiO_2 nano-rods, which indicates that TiO_2-NRs exposed (100) facet dominantly.

Raman results of TiO_2-NOs and TiO_2-NRs samples are showed in Fig. 2. Both TiO_2-NOs and TiO_2-NRs samples exhibit Raman peaks at 144, 394, 514, and 636 cm^{-1}, which are contribute to Eg, B1g, A1g, and Eg modes of TiO_2, respectively. A slight red shift of Raman peaks of TiO_2-NRs samples is observed comparing with that of TiO_2-NOs samples. According to literatures [49], Ti—O bands with band length of 198.3 and 193.0 nm exist in exposed (100) facet of TiO_2, whereas only Ti—O bands with band length of 193.0 nm exist in exposed (101) facet of TiO_2. (101) facet of TiO_2 has more lattice stress than (100) facet of TiO_2, which results in the Raman peaks red shift between TiO_2-NOs and TiO_2-NRs samples. It is further confirmed that TiO_2-NRs mainly expose

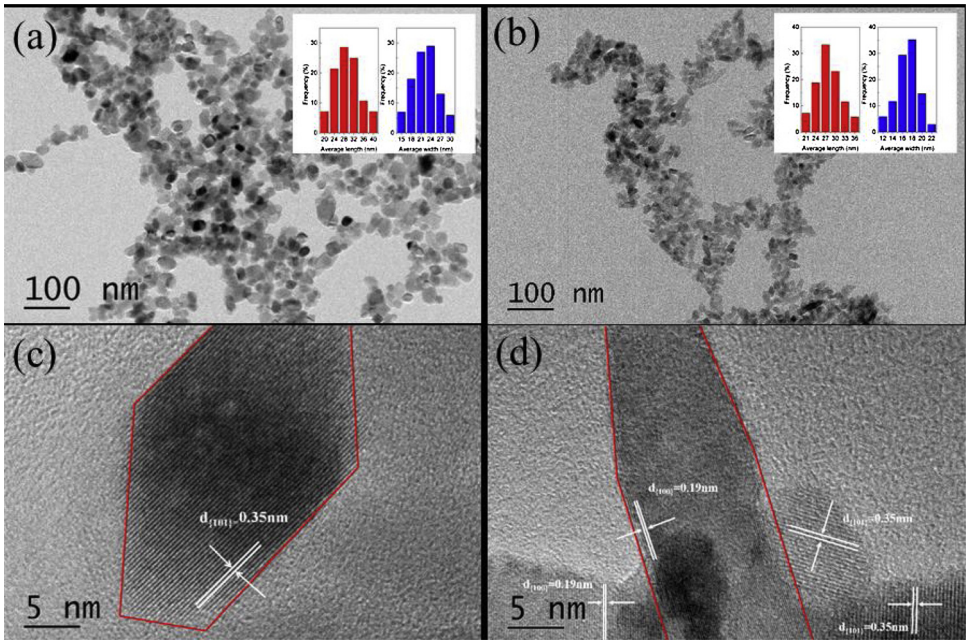

Fig. 1. TEM and HERTEM and simulation diagram of TiO_2-NOs and TiO_2-NRs: (a, c) TiO_2-NOs, (b, d) TiO_2-NRs.

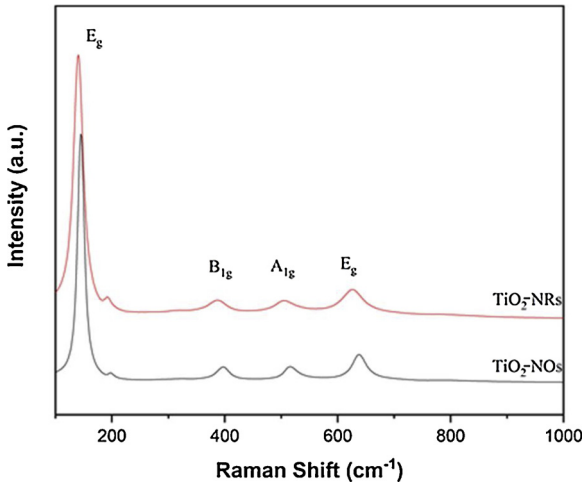

Fig. 2. Raman results of the TiO_2-NOs and TiO_2-NRs supports.

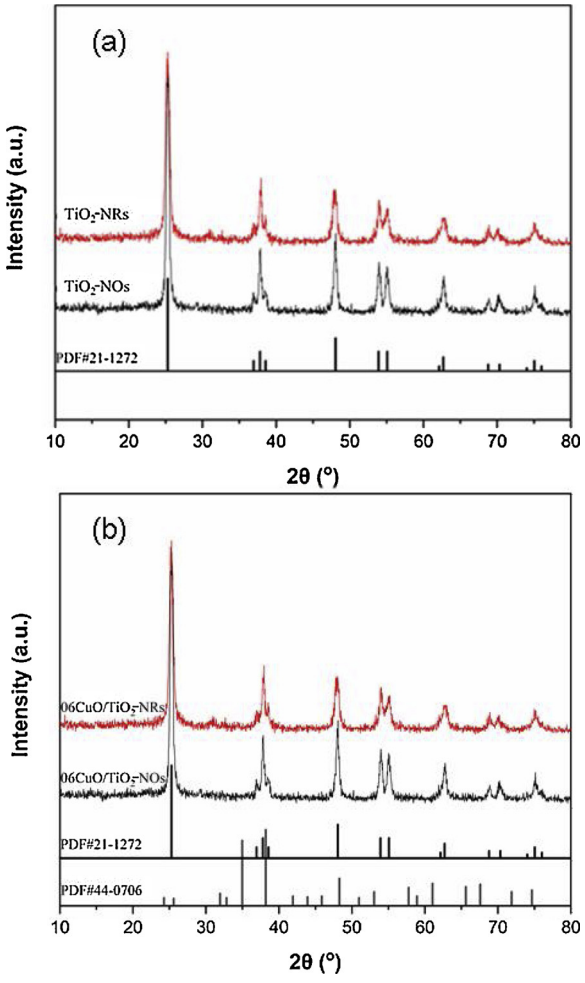

Fig. 3. XRD results of (a) TiO_2 supports and (b) 06CuO/TiO_2 catalysts.

(100) facet, and TiO_2-NOs expose (101) facet dominantly.

XRD results of TiO_2-NOs and TiO_2-NRs are displayed in Fig. 3a. Both TiO_2-NOs and TiO_2-NRs exhibit diffraction peaks at 25.3°, 36.9°, 37.8°, 48.1°, 53.9°, 55.0°, 62.1°, 62.7°, 68.8°, 70.3°, 74.0°, 75.0°, and 76.0°, corresponding to (101), (103), (004), (200), (105), (211), (213), (204), (116), (220), (107), (215), and (301) facets of anatase TiO_2 (PDF#21-1272). No peak of impurity is detected. It is indicated that both TiO_2-NOs and TiO_2-NRs are pure anatase TiO_2 phase.

In order to study CuO states on surfaces of 06CuO/TiO_2-NOs and 06CuO/TiO_2-NRs samples, XRD and TEM analysis were employed. As showed in Fig. 3b, both 06CuO/TiO_2-NOs and 06CuO/TiO_2-NRs exhibit diffraction peaks of anatase TiO_2 (PDF#21-1272). No peak of impurity or significantly peak shift is observed. It is indicated that CuO species are highly dispersed on the surface of TiO_2, and TiO_2 lattice is not doped by Cu species during the preparation process. As showed in Fig. S2, It is found that Cu species are highly dispersed on surface of TiO_2 supports. 06CuO/TiO_2-NOs and 06CuO/TiO_2-NRs exhibit octahedron and nano-rods shapes, respectively, which indicates that TiO_2 supports are stable during Cu species loading process. In addition, EDS mappings of 06CuO/TiO_2 catalysts are showed in Fig. S3. In case of both 06CuO/

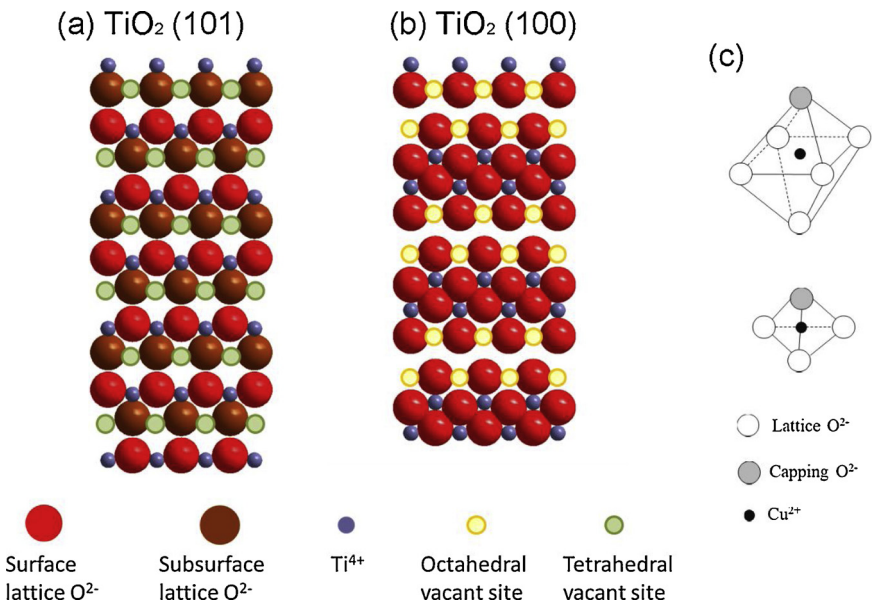

Fig. 4. Schematic diagram for TiO_2 with different exposed facets: (a)TiO_2 (101), (b) TiO_2 (100),and (c) Cu cation in octahedral vacant site and in tetrahedral vacant site.

TiO_2-NOs and 06CuO/TiO_2-NRs, EDS images of Cu and Ti match the HAADF image well. It is estimated that Cu species are highly dispersed on TiO_2 supports, which matches the XRD results.

According to incorporation model [46], the dispersion of various ionic compounds are proceeded by the incorporation of the metal cations into the surface vacant sites on the support, in which the loading amounts of the compounds are not higher than their dispersion capacities. The key factors determining the dispersion capacities of the ionic compounds are: (1) the surface structure of the support which determines the size and number of the vacant sites available; (2) the valency of the dispersed ionic compound and the size of the anion, from which the shielding effect of the capping anion(s) can be evaluated, and (3) the sizes of the dispersed cations and the vacant sites on the surface, from which the sites can be used for incorporation can be identified. In case of Cu^{2+} cations, the ion radius of Cu^{2+} ions is much smaller than that of O^{2-}, which makes Cu^{2+} ions can enter in both tetrahedral vacant sites and octahedral vacant sites of TiO_2. One Cu^{2+} cation needs a capping O^{2-} to balance the surface charge changing caused by Cu^{2+} loading. Therefore, the dispersion capacity of Cu^{2+} on (101) and (100) facets of TiO_2 can be estimated. As showed in Fig. 4, there are 2 tetrahedral vacant sites in each cell unit of exposed TiO_2 (101) facet, and exposed TiO_2 (100) facet has 2 octahedral vacant sites in each cell unit. In other words, exposed TiO_2 (101) facet has 0.86 mmol tetrahedral vacant sites per 100 m^2, and exposed TiO_2 (100) facet has 0.92 mmol octahedral vacant sites per 100 m^2 (Calculation details were showed in supporting information). Obviously, the amounts of loading CuO in 06CuO/TiO_2-NOs and 06CuO/TiO_2-NRs samples are lower than their dispersion capacities on TiO_2-NOs and TiO_2-NRs. Therefore, Cu species are highly dispersed on the surface of TiO_2-NOs and TiO_2-NRs, which matches the XRD results.

3.2. NH_3-SCR performances of 06CuO/TiO_2-NOs and 06CuO/TiO_2-NRs

Here the structures of 06CuO/TiO_2-NOs and 06CuO/TiO_2-NRs are clear. NH_3-SCR performances of 06CuO/TiO_2-NOs and 06CuO/TiO_2-NRs are further investigated. As it is showed in Fig. 5, NO conversions of 06CuO/TiO_2-NOs and 06CuO/TiO_2-NRs offer upgrade firstly then descending latter tendency at the temperature range from 150 °C to 450 °C. 06CuO/TiO_2-NOs exhibits the highest NO conversions at 275 °C, whereas the NO conversions of 06CuO/TiO_2-NRs reach its maximum at 400 °C. When the reaction temperature is lower than 325 °C, NH_3-SCR

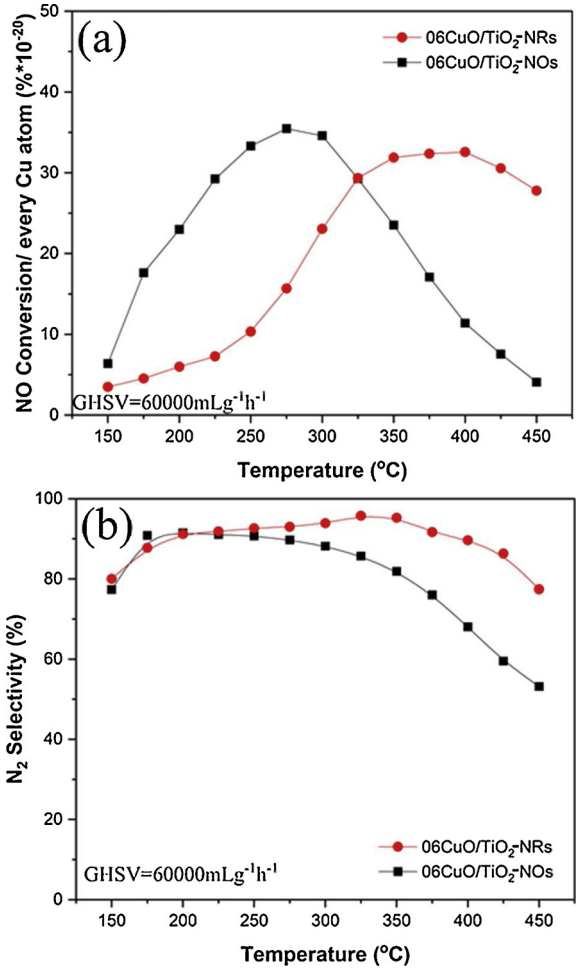

Fig. 5. Results of normalized (a) NO conversion and (b) N_2 selectivity.

performance of 06CuO/TiO_2-NOs surpasses that of 06CuO/TiO_2-NRs. N_2 selectivity of 06CuO/TiO_2-NOs and 06CuO/TiO_2-NRs are showed in Fig. 5b. Both 06CuO/TiO_2-NOs and 06CuO/TiO_2-NRs exhibit N_2

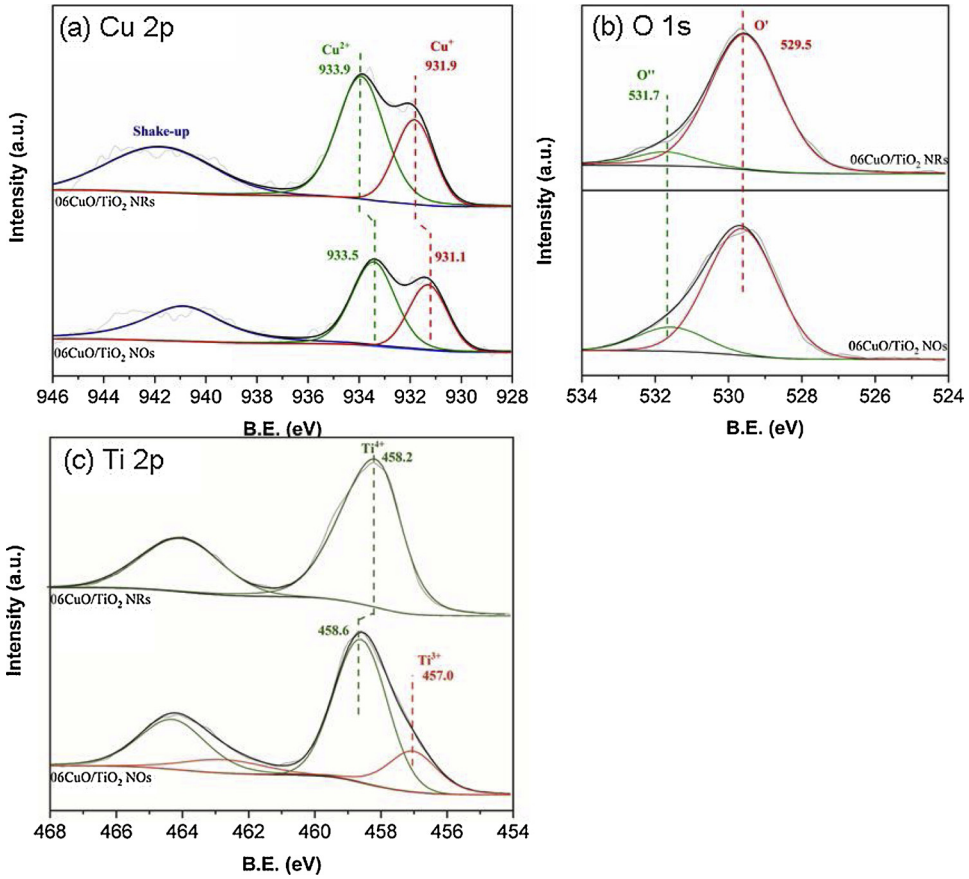

Fig. 6. XPS results of 06CuO/TiO_2-NOs and 06CuO/TiO_2-NRs: (a) Cu 2p, (b) O 1s, (c) Ti 2p.

selectivity over 90%, whereas their N_2 selectivity gradually decrease when reaction temperatures increase. When temperature is over 250 °C, N_2 selectivity of 06CuO/TiO_2-NOs declines more quickly than that of 06CuO/TiO_2-NRs. N_2 selectivity of 06CuO/TiO_2-NRs maintains over 80% when temperature reaches 450 °C, whereas that of 06CuO/TiO_2-NOs decreases to 50%. Obviously, different exposed facets of TiO_2 support have significant effect on NH_3-SCR performances of 06CuO/TiO_2.

3.3. Relationship between catalyst structures and catalytic performances

In order to understand the relationship between exposed facets of TiO_2 support and the NH_3-SCR performances of 06CuO/TiO_2-NOs and 06CuO/TiO_2-NRs samples, XPS, NH_3-TPD, and H_2-TPR analysis were employed.

Surface element states were investigated by XPS analysis, and the results are showed in Fig. 6. O1s peaks of catalysts can be divided as two peaks centered at 529.5 and 531.7 eV. The fined peak at 529.5 eV (O') is contributed to lattice oxygen, and another fined peak at 531.7 (O") is corresponded to adsorbed oxygen [21]. According to Ettireddy's report [50], O_2 in air could be activated by oxygen vacancies on catalyst surfaces, and thus participates in NH_3-SCR. More surface adsorbed oxygen is beneficial to NH_3-SCR on metal oxide catalysts. In addition, increasing surface adsorbed oxygen could accelerate the transformation from NO to NO_2, which could enhance low temperature NH_3-SCR activity. The relative surface oxygen concentration is calculated, and the results are showed in Table 1. Obviously, 06CuO/TiO_2-NOs has more adsorbed oxygen than 06CuO/TiO_2-NRs, which matches with their NH_3-SCR performances lower than 325 °C. In XPS spectra of Cu 2p, peaks of Cu^+ and Cu^{2+}, peaks centered at 931.9 eV and 933.9 eV are detected. [32] 06CuO/TiO_2-NOs exhibits more surface Cu^+ species than 06CuO/TiO_2-NRs (Table 1). Besides, Cu^+ peak of 06CuO/TiO_2-NOs shifts to lower binding energy side than that of 06CuO/TiO_2-NRs, which indicates that Cu^+ species on the surface of 06CuO/TiO_2-NOs have less positive charge. In Ti 2p spectra of 06CuO/TiO_2-NOs, Ti^{4+} at 458.6 eV and Ti^{3+} at 457.0 eV are detected, [51] whereas only Ti^{4+} species can be detected in XPS spectra of 06CuO/TiO_2-NRs. Moreover, Ti^{4+} peak of 06CuO/TiO_2-NOs moves to higher binding energy side than that of 06CuO/TiO_2-NRs, which indicates that Ti^{4+} species on the surface of 06CuO/TiO_2-NOs have more positive charge. According to the catalyst structure analysis mentioned before, (101) facet of TiO_2, which is mainly exposed in 06CuO/TiO_2-NOs, has only tetrahedral vacant sites, whereas (100) facet of TiO_2 has only octahedral vacant sites. Therefore, Cu cation locates in tetrahedral vacant sites on (101) facet of TiO_2, and locates in octahedral vacant sites on (100) facet of TiO_2. As showed in Fig. 4c, Cu cation in tetrahedral vacant sites is coordinated by 4 neighbor oxygen, and the distance between Cu and neighbor Ti is lower than the case Cu located in octahedral vacant sites. It is reasonable to infer that, Cu cation in tetrahedral vacant sites has strong interaction with exposed TiO_2 (101) facet of 06CuO/TiO_2-NOs, so that electron can transmit from Ti to Cu, which results in the XPS peaks shift phenomena of 06CuO/TiO_2-NOs. Moreover, the strong interaction between Cu and TiO_2 (101) facet is beneficial to $Cu^{2+} + Ti^{3+} \longleftrightarrow Cu^{+} + Ti^{4+}$ cycle. According to literatures [52], the

Table 1
Surface atomic distributions of the 06CuO/TiO_2 catalysts by XPS.

Sample	Atomic ratio/%		
	O' / (O' + O")	Cu^+ / (Cu^+ + Cu^{2+})	Ti^{3+} / (Ti^{3+} + Ti^{4+})
06CuO/TiO_2-NRs	9.0	34.2	–
06CuO/TiO_2-NOs	15.9	39.1	18.7

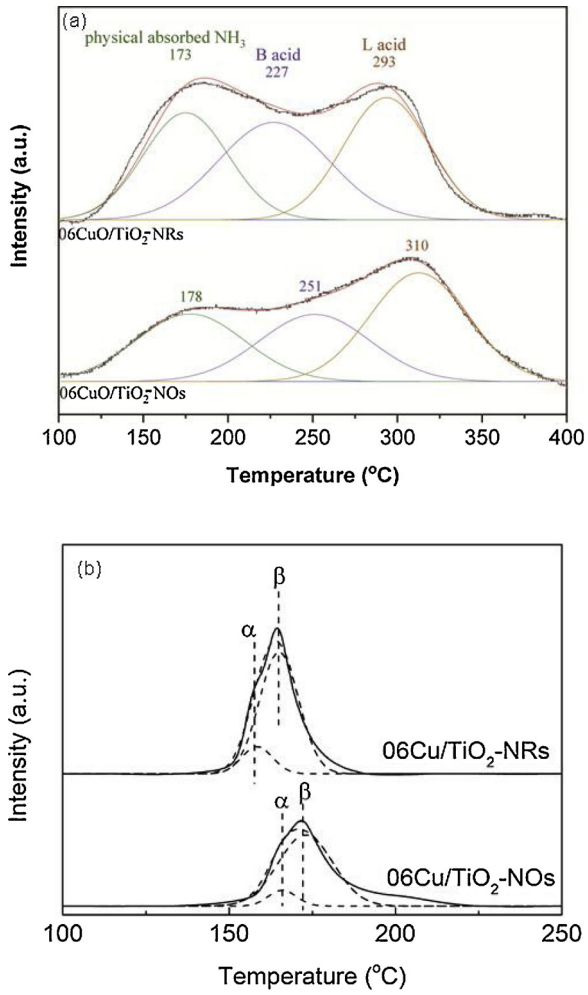

Fig. 7. (a) NH_3-TPD and (b) H_2-TPR results of 06CuO/TiO_2 catalysts.

oxidation reduction cycle on catalysts could not only enhance the redox ability of catalyst, but also introduce more acid sites, which are beneficial to NH_3-SCR on catalyst.

Acidity of catalysts, which can influence the absorption of reaction agents, is an important fact affect the NH_3-SCR performance of catalysts. This property of catalysts were investigated by NH_3-TPD analysis. As showed in Fig. 7a, both 06CuO/TiO_2-NOs and 06CuO/TiO_2-NRs exhibits NH_3 desorption signal from 100 to 400 °C. The total NH_3 desorption could be fined as an overlap of 3 divided peaks centered at 175, 250, and 300 °C. According to literatures, [53] desorption peak at 175 °C belongs to physical adsorbed NH_3. Peak at 250 °C is contributed to NH_3 adsorbed on Bronsted acid sites, and Peak at 300 °C is corresponded to NH_3 adsorbed on Lewis acid sites. It is noteworthy that NH_3 desorption peaks belonged to Bronsted acid sites and Lewis acid sites of 06CuO/TiO_2-NOs shift to high temperature side than that of 06CuO/TiO_2-NRs. It is indicated that 06CuO/TiO_2-NOs has stronger acidity than 06CuO/TiO_2-NRs. Moreover, total acid contents of catalysts are calculated by NH_3 desorption peak areas, and are normalized by surface areas of 06CuO/TiO_2. In results, total acid content of 06CuO/TiO_2-NOs surpasses that of 06CuO/TiO_2-NRs, which verifies the conjecture mentioned in XPS analysis. The strong interaction between Cu in tetrahedral vacant sites and TiO_2 (101) facet cause the redox cycle $Cu^{2+} + Ti^{3+} \longleftrightarrow Cu^{+} + Ti^{4+}$. The existence of redox cycle $Cu^{2+} + Ti^{3+} \longleftrightarrow Cu^{+} + Ti^{4+}$ enhances the acidity and acid content of 06CuO/TiO_2-NOs.

The redox ability of materials is another significant fact which influences the catalytic activity of NH_3-SCR catalyst. H_2-TPR was utilized to discuss this property of the synthesized catalysts. As illustrated in Fig. 7b, both 06CuO/TiO_2-NOs and 06CuO/TiO_2-NRs exhibit similar two-peak behavior. H_2 consumption peaks α and β are a result of the two step reduction from $Cu^{2+} \rightarrow Cu^{+}$ and $Cu^{+} \rightarrow Cu^{\circ}$ [54]. The total H_2 consumption is normalized by surface area of catalyst, and the results are showed in Table S2. It is found that the normalized H_2 consumption of 06CuO/TiO_2-NOs and 06CuO/TiO_2-NRs are similar, which indicates the close redox property of these two catalysts. Therefore, in 06CuO/TiO_2 system, the redox ability of catalysts is not the main reason effected on the NH_3-SCR performances.

NH_3 adsorption curves of 06CuO/TiO_2 catalysts are showed in Fig. 8. IR peaks at 1160, 1230, 1294, 1600, and 1650 cm^{-1} are

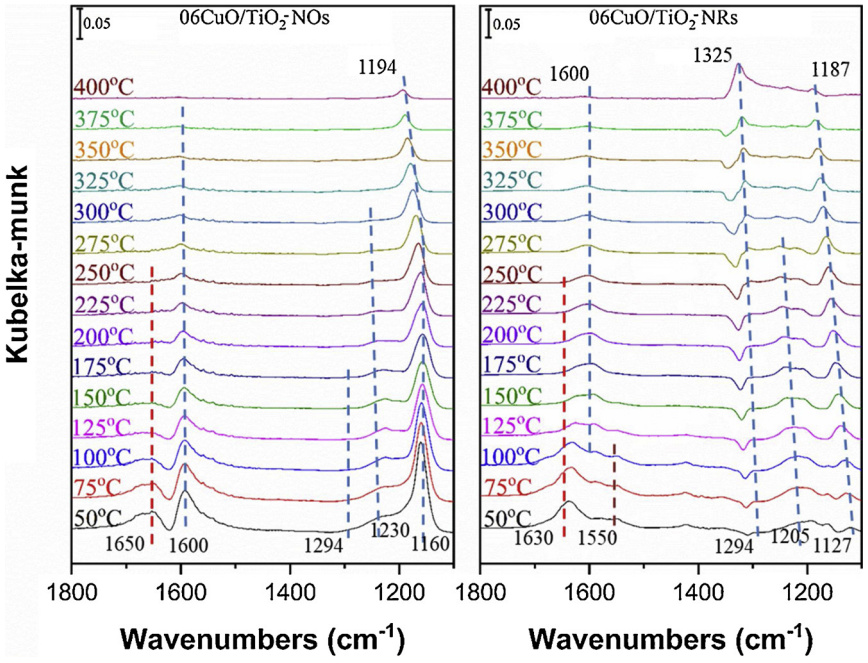

Fig. 8. In-situ DRIFTS results of NH_3 adsorption and desorption on the 06CuO/TiO_2 catalysts surface with temperature increasing.

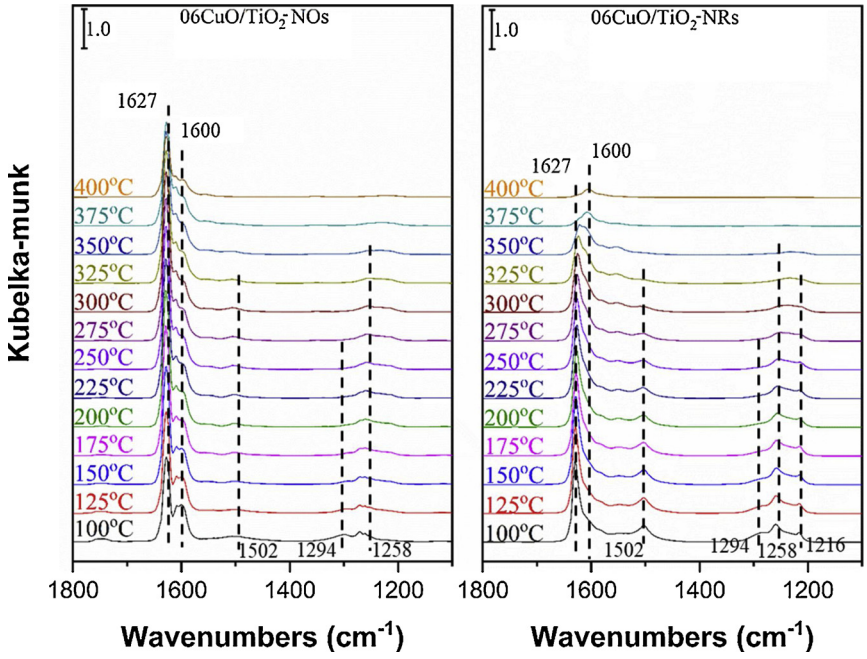

Fig. 9. In-situ DRIFTS results of $NO + O_2$ adsorption and desorption on the $06CuO/TiO_2$ catalysts surface with temperature increasing.

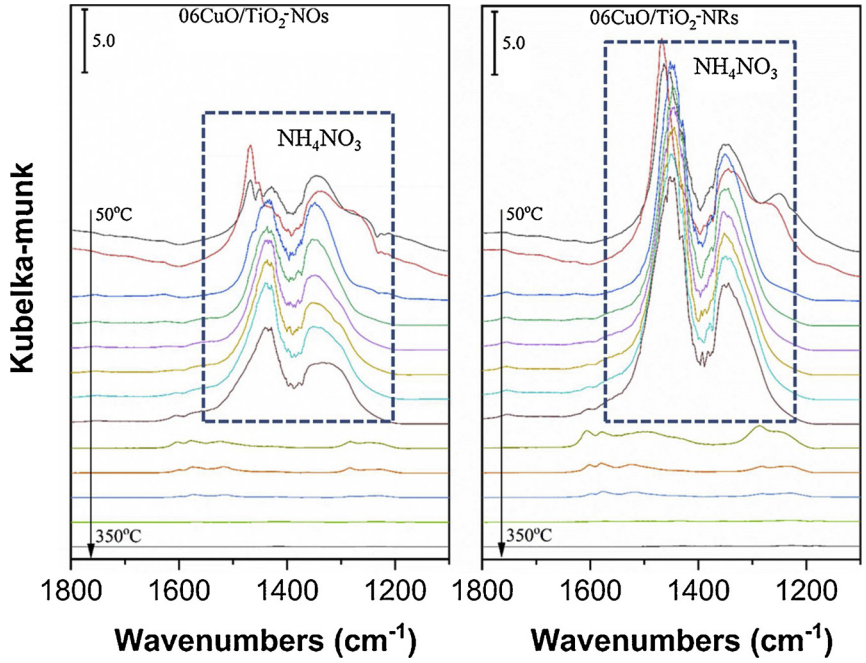

Fig. 10. In-situ DRIFTS results of $NH_3 + NO + O_2$ absorption and desorption on the $06CuO/TiO_2$ catalysts surface with temperature increasing.

detected. They are contributed to NH_3 adsorbed on Bronsted acid sites (1650 cm^{-1}) and Lewis acid sites on catalysts (1600, 1294, 1230, and 1160 cm^{-1}), respectively [55,56]. At low temperature (< 325 °C), IR peaks of NH_3 adsorbed on Lewis acid sites of $06CuO/TiO_2$-NOs is higher than that of $06CuO/TiO_2$-NRs. It is indicated that Lewis acid content of $06CuO/TiO_2$-NOs surpasses that of $06CuO/TiO_2$-NRs, which matches NH_3-TPD results. It is reasonable to infer that the enhanced acidity of $06CuO/TiO_2$-NOs promotes the NH_3-SCR performance on it.

$NO + O_2$ co-adsorption curves on $06CuO/TiO_2$ catalysts are showed in Fig. 9. IR peaks at 1216, 1258, 1294, 1502, 1600, and 1627 cm^{-1} are detected in $NO + O_2$ co-adsorption curves at 100 °C. According to literatures, IR peaks at 1216 and 1258 cm^{-1} belong to bridge nitrate; IR peaks at 1294 cm^{-1} belong to monodentate nitrate; IR peaks at 1502 cm^{-1} belong to liner nitrite; IR peaks at 1600 and 1627 cm^{-1} belong to bidentate nitrate [57,58]. With temperature increasing, IR peaks of bridge nitrate, liner nitrite, and monodentate nitrate gradually disappear. However, bidentate nitrate is stable. The intensities of IR peaks of bidentate nitrate on $06CuO/TiO_2$-NOs are strong at 400 °C, whereas that of $06CuO/TiO_2$-NRs significantly decrease and disappear when temperature is over 325 °C. The stable bidentate nitrate occupies metal sites on catalyst surfaces, which might results in the lower NH_3-SCR performances of $06CuO/TiO_2$-NOs than $06CuO/TiO_2$-NRs when temperature is over 325 °C.

$NH_3 + NO + O_2$ co-adsorption on $06CuO/TiO_2$ catalysts were further investigated, and the result is showed in Fig. 10. No peak of bidentate nitrate is detected in both $NH_3 + NO + O_2$ co-adsorption curves

of 06CuO/TiO_2-NOs and 06CuO/TiO_2-NRs. According to literatures, NH_3 and NO competitively adsorb on catalyst surfaces. In results, one of O−M band of bridge nitrate breaks, forming coordinated NH_3 and a monodentate nitrate. The nearby coordinated NH_3 and monodentate nitrate further transform to NH_4NO_3 covered on surface of catalyst. [59] Obviously, NH_4NO_3 on surface of 06CuO/TiO_2-NRs is much more than that on the surface of 06CuO/TiO_2-NOs, at low temperature. NH_4NO_3 covers the active sites of catalysts, which inhibits NH_3-SCR on catalyst. Therefore, 06CuO/TiO_2-NOs exhibits better NH_3-SCR performances than 06CuO/TiO_2-NRs. When temperature increase, NH_4NO_3 gradually decomposes and disappears form surface of catalysts. Hence, the covered NH_4NO_3 hardly influences NH_3-SCR performances of 06CuO/TiO_2 at high temperature.

4. Conclusions

In this work, CuO loading TiO_2 nano-octahedron (06CuO/TiO_2-NOs) and CuO loading TiO_2 nano-rods (06CuO/TiO_2-NRs) were synthesized. By modifying the morphology of TiO_2 support, the effects of TiO_2 exposed facet on NH_3-SCR performances were investigated. In results, TiO_2-NOs and TiO_2-NRs expose (101) and (100) facets of TiO_2, respectively. In case of these two TiO_2 expose different facets, the location of Cu cations on their surfaces are different. Cu cations locate in tetrahedral vacant sites on TiO_2 (101) facets, whereas it locate in octahedral vacant sites on TiO_2 (100) facets. The different coordination environments bring the different NH_3-SCR performances. In case of 06CuO/TiO_2-NOs, Cu cations in tetrahedral vacant sites is coordinated by 4 neighbor oxygen. The distance from Cu cations to neighbor Ti is shorter than that of Cu cations in 06CuO/TiO_2-NRs, which is coordinated by 6 neighbor oxygen. Therefore, Cu cations in 06CuO/TiO_2-NOs exhibit strong interaction with exposed TiO_2 (101) facets, which results in redox cycle $Cu^{2+} + Ti^{3+} \longleftrightarrow Cu^{+} + Ti^{4+}$ on the surface of 06CuO/TiO_2-NOs. The redox cycle enhances the redox ability of catalyst, and introduces more acid sites, which is beneficial to NH_3-SCR on catalyst. In addition, NH_4NO_3 is easy to form and deposit on surface of TiO_2-NRs at low temperature, which further decreases the NH_3-SCR performance of TiO_2-NRs.

Acknowledgements

The financial supports of National Natural Science Foundation of China (No. 21573105), Natural Science Foundation of Jiangsu Province (BK20161392) are gratefully acknowledged.

References

[1] P. Forzatti, Present status and perspectives in de-NOx SCR catalysis, Appl. Catal. A-Gen. 222 (2001) 221–236.
[2] G.S. Qi, R.T. Yang, R. Chang, MnOx-CeO_2 mixed oxides prepared by co-precipitation for selective catalytic reduction of NO with NH_3 at low temperatures, Appl. Catal. B-Environ. 51 (2004) 93–106.
[3] P.G. Smirniotis, D.A. Peña, B.S. Uphade, Selektive katalytische reduktion von NO durch NH_3 bei niedrigen temperaturen mit Hilfe von Mn-, Cr-und Cu-Oxiden auf einem Hombikat-TiO_2-Träger, Angew. Chemie 113 (2001) 2537–2540.
[4] T. Boningari, P.G. Smirniotis, Impact of nitrogen oxides on the environment and human health: Mn-based materials for the NOx abatement, Curr. Opin. Chem. Eng. 13 (2016) 133–141.
[5] D.W. Fickel, E. D'Addio, J.A. Lauterbach, R.F. Lobo, The ammonia selective catalytic reduction activity of copper-exchanged small-pore zeolites, Appl. Catal. B-Environ. 102 (2011) 441–448.
[6] S. Brandenberger, O. Kroecher, A. Tissler, R. Althoff, The state of the art in selective catalytic reduction of NOx by ammonia using metal-exchanged zeolite catalysts, Catal. Rev.-Sci. Eng. 50 (2008) 492–531.
[7] M. Kang, E.D. Park, J.M. Kim, J.E. Yie, Cu-Mn mixed oxides for low temperature NO reduction with NH_3, Catal. Today 111 (2006) 236–241.
[8] U. Deka, A. Juhin, E.A. Eilertsen, H. Emerich, M.A. Green, S.T. Korhonen, B.M. Weckhuysen, A.M. Beale, Confirmation of isolated Cu^{2+} ions in SSZ-13 zeolite as active sites in NH_3-selective catalytic reduction, J. Phys. Chem. C 116 (2012) 4809–4818.
[9] D. Damma, T. Boningari, P.R. Ettireddy, B.M. Reddy, P.G. Smirniotis, Direct decomposition of NOx over TiO_2 supported transition metal oxides at low temperatures, Ind. Eng. Chem. Res. 57 (2018) 16615–16621.
[10] M. Kang, E.D. Park, J.M. Kim, J.E. Yie, Manganese oxide catalysts for NOx reduction with NH_3 at low temperatures, Appl. Catal. A-Gen. 327 (2007) 261–269.
[11] G.S. Qi, R.T. Yang, Performance and kinetics study for low-temperature SCR of NO with NH_3 over MnOx-CeO_2 catalyst, J. Catal. 217 (2003) 434–441.
[12] J. Tan, Y. Wei, Y. Sun, J. Liu, Z. Zhao, W. Song, J. Li, X. Zhang, Simultaneous removal of NOx and soot particulates from diesel engine exhaust by 3DOM Fe-Mn oxide catalysts, J. Ind. Eng. Chem. (Amsterdam, Neth.) 63 (2018) 84–94.
[13] D.K. Pappas, T. Boningari, P. Boolchand, P.G. Smirniotis, Novel manganese oxide confined interweaved titania nanotubes for the low-temperature Selective Catalytic Reduction (SCR) of NOx by NH_3, J. Catal. 334 (2016) 1–13.
[14] T. Boningari, D.K. Pappas, P.R. Ettireddy, A. Kotrba, P.G. Smirniotis, Influence of SiO_2 on M/TiO_2 (M = Cu, Mn, and Ce) formulations for low-temperature selective catalytic reduction of NOx with NH_3: surface properties and key components in relation to the activity of NOx reduction, Ind. Eng. Chem. Res. 54 (2015) 2261–2273.
[15] E.T.C. Vogt, A. van Dillen, J.W. Geus, F.J.J.G. Janssen, Selective catalytic reduction of NOx with NH_3 over a V_2O_5/TiO_2 on silica catalyst, Catal. Today 2 (1988) 569–579.
[16] L.J. Alemany, L. Lietti, N. Ferlazzo, P. Forzatti, G. Busca, E. Giamello, F. Bregani, Reactivity and physicochemical characterization of V_2O_5-WO_3/TiO_2 de-NOx catalysts, J. Catal. 155 (1995) 117–130.
[17] N.Y. Topsoe, H. Topsoe, J.A. Dumesic, Vanadia-titania catalysts for selective catalytic reduction (SCR) of nitric-oxide by ammonia. 1. Combined temperature-programmed in-situ FTIR and online mass-spectroscopy studies, J. Catal. 151 (1995) 226–240.
[18] F. Liu, H. He, Y. Ding, C. Zhang, Effect of manganese substitution on the structure and activity of iron titanate catalyst for the selective catalytic reduction of NO with NH_3, Appl. Catal. B-Environ. 93 (2009) 194–204.
[19] S. Yang, C. Wang, J. Li, N. Yan, L. Ma, H. Chang, Low temperature selective catalytic reduction of NO with NH_3 over Mn-Fe spinel: performance, mechanism and kinetic study, Appl. Catal. B-Environ. 110 (2011) 71–80.
[20] A. Grossale, I. Nova, E. Tronconi, D. Chatterjee, M. Weibel, The chemistry of the NO/NO_2-NH_3 "fast" SCR reaction over Fe-ZSM5 investigated by transient reaction analysis, J. Catal. 256 (2008) 312–322.
[21] Z. Wu, R. Jin, Y. Liu, H. Wang, Ceria modified MnOx/TiO_2 as a superior catalyst for NO reduction with NH_3 at low-temperature, Catal. Commun. 9 (2008) 2217–2220.
[22] T. Boningari, P.R. Ettireddy, A. Somogyvari, Y. Liu, A. Vorontsov, C.A. McDonald, P.G. Smirniotis, Influence of elevated surface texture hydrated titania on Ce-doped Mn/TiO_2 catalysts for the low-temperature SCR of NOx under oxygen-rich conditions, J. Catal. 325 (2015) 145–155.
[23] J. Xu, G. Chen, F. Guo, J. Xie, Development of wide-temperature vanadium-based catalysts for selective catalytic reducing of NOx with ammonia: review, Chem. Eng. J. 353 (2018) 507–518.
[24] J. Zhang, X. Li, P. Chen, B. Zhu, Research status and prospect on vanadium-based catalysts for NH_3-SCR denitration, Materials 11 (2018).
[25] F. Liu, W. Shan, X. Shi, H. He, Vanadium-based catalysts for the selective catalytic reduction of NOx with NH_3, Prog. Chem. 24 (2012) 445–455.
[26] C. Gao, J.-W. Shi, Z. Fan, G. Gao, C. Niu, Sulfur and water resistance of Mn-based catalysts for low-temperature selective catalytic reduction of NOx: a review, Catalysts 8 (2018).
[27] G. Li, B. Wang, J. Ma, J. Zhou, Y. Li, W. Xu, Y. Han, Q. Sun, Manganese-based molecular sieve catalysts for low-temperature NH_3-SCR, Huanjing Huaxue-Environ. Chem. 37 (2018) 769–781.
[28] J. Zhou, B. Wang, J. Ma, G. Li, Q. Sun, W. Xu, Y. Li, SO_2 and H_2O poisoning resistance of manganese oxide-based catalysts for low-temperature selective catalytic reduction of NOx, Huanjing Huaxue-Environ. Chem. 37 (2018) 782–791.
[29] Z. Chen, C. Fan, L. Pang, S. Ming, P. Liu, T. Li, The influence of phosphorus on the catalytic properties, durability, sulfur resistance and kinetics of Cu-SSZ-13 for NOx reduction by NH_3-SCR, Appl. Catal. B-Environ. 237 (2018) 116–127.
[30] L. Bing, G. Wang, K. Yi, A. Tian, F. Wang, C. Wu, One-pot synthesis of Cu-SAPO-34 catalyst using waste mother liquid and its application in the selective catalytic reduction of NO with NH_3, Catal. Today 316 (2018) 37–42.
[31] Y. Cao, D. Fan, P. Tian, L. Cao, T. Sun, S. Xu, M. Yang, Z. Liu, The influence of low-temperature hydration methods on the stability of Cu-SAPO-34 SCR catalyst, Chem. Eng. J. 354 (2018) 85–92.
[32] Z. Si, D. Weng, X. Wu, Y. Jiang, B. Wang, Synergistic effects between copper and tungsten on the structural and acidic properties of CuOx/WOx-ZrO_2 catalyst, Catal. Sci. Technol. 1 (2011) 453–461.
[33] J.A. Sullivan, J.A. Doherty, NH_3 and urea in the selective catalytic reduction of NOx over oxide-supported copper catalysts, Appl. Catal. B-Environ. 55 (2005) 185–194.
[34] J.A. Sullivan, The effect of support and Cu precursor on the activity of supported CuO catalysts in the selective catalytic reduction of NOx, Catal. Lett. 79 (2002) 59–62.
[35] X. Wu, Y. Feng, Y. Du, X. Liu, C. Zou, Z. Li, Enhancing DeNOx performance of CoMnAl mixed metal oxides in low-temperature NH_3-SCR by optimizing layered double hydroxides (LDHs) precursor template, Appl. Surf. Sci. 467 (2019) 802–810.
[36] S. Ali, L. Chen, Z. Li, T. Zhang, R. Li, S.u.H. Bakhtiar, X. Leng, F. Yuan, X. Niu, Y. Zhu, Cu_xNb_{1-x} (x = 0.45, 0.35, 0.25, 0.15) bimetal oxides catalysts for the low temperature selective catalytic reduction of NO with NH_3, Appl. Catal. B-Environ. 236 (2018) 25–35.
[37] Y. Wei, X. Wu, Y. Zhao, L. Wang, Z. Zhao, X. Huang, J. Liu, J. Li, Efficient photocatalysts of TiO_2 nanocrystals-supported PtRu alloy nanoparticles for CO_2 reduction with H_2O: synergistic effect of Pt-Ru, Appl. Catal. B-Environ. 236 (2018) 445–457.
[38] Y. Zhao, Y. Wei, X. Wu, H. Zheng, Z. Zhao, J. Liu, J. Li, Graphene-wrapped Pt/TiO_2 photocatalysts with enhanced photogenerated charges separation and reactant

adsorption for high selective photoreduction of CO_2 to CH_4, Appl. Catal. B-Environ. 226 (2018) 360–372.
[39] L. Song, R. Zhang, S. Zang, H. He, Y. Su, W. Qiu, X. Sun, Activity of selective catalytic reduction of NO over V_2O_5/TiO_2 catalysts preferentially exposed anatase {001} and {101} facets, Catal. Lett. 147 (2017) 934–945.
[40] S. Deng, T. Meng, B. Xu, F. Gao, Y. Ding, L. Yu, Y. Fan, Advanced MnOx/TiO_2 catalyst with preferentially exposed anatase {001} facet for low-temperature SCR of NO, ACS Catal. 6 (2016) 5807–5815.
[41] Q. Shi, Y. Li, Y. Zhou, S. Miao, N. Ta, E. Zhan, J. Liu, W. Shen, The shape effect of TiO_2 in VOx/TiO_2 catalysts for selective reduction of NO by NH_3, J. Mater. Chem. A 3 (2015) 14409–14415.
[42] Y. Lv, H. Zhang, X. Yao, L. Dong, Y. Chen, Investigation of the physicochemical properties of CuO/Sm_2O_3/gamma-Al_2O_3 catalysts and their activity for NO removal by CO, J. Mol. Catal. A-Chem. 420 (2016) 34–44.
[43] J. Sun, L. Zhang, C. Ge, C. Tang, L. Dong, Comparative study on the catalytic CO oxidation properties of CuO/CeO_2 catalysts prepared by solid state and wet impregnation, Chin. J. Catal. 35 (2014) 1347–1358.
[44] Y. Xiong, X. Yao, C. Tang, L. Zhang, Y. Cao, Y. Deng, F. Gao, L. Dong, Effect of CO-pretreatment on the CuO-V_2O_5/gamma-Al_2O_3 catalyst for NO reduction by CO, Catal. Sci. Technol. 4 (2014) 4416–4425.
[45] B. Xu, L. Dong, Y. Chen, Influence of CuO loading on dispersion and reduction behavior of CuO/TiO_2 (anatase) system, J. Chem. Soc.-Faraday Trans. 94 (1998) 1905–1909.
[46] Y. Chen, L. Dong, Y.S. Jin, B. Xu, W.J. Ji, Studies on Supported Metal Oxide-Oxide Support Interactions (An Incorporation Model), (1996).
[47] L. Dong, Z. Liu, Y.H. Hu, B. Xu, Y. Chen, Dispersion and reduction behavior of CuO/alpha-Fe_2O_3 systems, J. Chem. Soc.-Faraday Trans. 94 (1998) 3033–3038.
[48] L. Liu, X. Gu, Z. Ji, W. Zou, C. Tang, F. Gao, L. Dong, Anion-assisted synthesis of TiO_2 nanocrystals with tunable crystal forms and crystal facets and their photocatalytic redox activities in organic reactions, J. Phys. Chem. C 117 (2013) 18578–18587.
[49] F. Tian, Y. Zhang, J. Zhang, C. Pan, Raman spectroscopy: a new approach to measure the percentage of anatase TiO_2 exposed (001) facets, J. Phys. Chem. C 116 (2012) 7515–7519.
[50] P.R. Ettireddy, N. Ettireddy, S. Mamedov, P. Boolchand, P.G. Smirniotis, Surface characterization studies of TiO_2 supported manganese oxide catalysts for low temperature SCR of NO with NH_3, Appl. Catal. B-Environ. 76 (2007) 123–134.
[51] X. Gao, Y. Jiang, Y. Zhong, Z. Luo, K. Cen, The activity and characterization of CeO_2-TiO_2 catalysts prepared by the sol-gel method for selective catalytic reduction of NO with NH_3, J. Hazard. Mater. 174 (2010) 734–739.
[52] X.W. Li, M.M. Shen, H. Xi, H.Y. Zhu, F. Gao, K. Yan, D. Lin, C. Yi, Dispersion and reduction of copper oxide supported on WO_3-modified $Ce_{0.5}Zr_{0.5}O_2$ solid solution, J. Phys. Chem. B 109 (2005) 3949–3955.
[53] B. Jiang, B. Deng, Z. Zhang, Z. Wu, X. Tang, S. Yao, H. Lu, Effect of Zr addition on the low-temperature SCR activity and SO_2 tolerance of Fe-Mn/Ti catalysts, J. Phys. Chem. C 118 (2014) 14866–14875.
[54] Y.H. Hu, L. Dong, J. Wang, W.P. Ding, Y. Chen, Activities of supported copper oxide catalysts in the NO plus CO reaction at low temperatures, J. Mol. Catal. A-Chem. 162 (2000) 307–316.
[55] W. Shan, F. Liu, H. He, X. Shi, C. Zhang, Novel cerium-tungsten mixed oxide catalyst for the selective catalytic reduction of NOx with NH_3, Chem. Commun. 47 (2011) 8046–8048.
[56] N.Y. Topsoe, Mechanism of the selective catalytic reduction of nitric-oxide by ammonia elucidated by in-situ online fourier-transform infrared-spectroscopy, Science 265 (1994) 1217–1219.
[57] Z. Wu, B. Jiang, Y. Liu, H. Wang, R. Jin, DRIFT study of manganese/titania-based catalysts for low-temperature selective catalytic reduction of NO with NH_3, Environ. Sci. Technol. 41 (2007) 5812–5817.
[58] H. Hu, S. Cai, H. Li, L. Huang, L. Shi, D. Zhang, In situ DRIFTs investigation of the low-temperature reaction mechanism over Mn-doped Co_3O_4 for the selective catalytic reduction of NOx with NH_3, J. Phys. Chem. C 119 (2015) 22924–22933.
[59] D. Meng, W. Zhan, Y. Guo, Y. Guo, L. Wang, G. Lu, A highly effective catalyst of Sm-MnOx for the NH_3-SCR of NOx at low temperature: promotional role of Sm and its catalytic performance, ACS Catal. 5 (2015) 5973–5983.